Fabrication of zinc ferrite ($ZnFe_2O_4$) as a photoanode layer on dye-sensitized solar cells from *Spirulina platensis*

[1]Razali Thaib, [1]Hamdani Umar, [2]Mulia S. Sari, [3]Rachmad A. Putra

[1] Mechanical Engineering Department, Faculty of Engineering, Universitas Syiah Kuala, Aceh, Indonesia; [2] Biology Study Program, Faculty of Engineering, Universitas Samudra, Aceh, Indonesia, [3] Physics Study Program, Faculty of Engineering, Universitas Samudra, Aceh, Indonesia. Corresponding author: R. Thaib, razalithaib@usk.ac.id

Abstract. Semiconductor materials are widely used in the construction of solar cells and dye-sensitized solar cells (DSSC). Subsequently, DSSC, a unique type of solar cell, operates on photoelectrochemical principles, facilitating the transfer of electrons between distinct phases. In comparison to conventional solar cells, DSSC stands out due to its separate charge separation and light absorption processes. Therefore, this research aimed to evaluate the potential of zinc ferrite ($ZnFe_2O_4$) as a substrate in DSSC technology. The dye material utilized was extracted from *Spirulina platensis* chlorophyll. The resulting $ZnFe_2O_4$ photoanode material exhibited polycrystalline properties, with a crystallite size ranging from 11.73 nm to 22.21 nm. The energy gap observed in this material ranges from 1.78 to 1.79 eV, indicating its suitability as a photoanode material for the DSSC configuration. The UV-Vis characterization results showed that soaking $ZnFe_2O_4$ with dye for 3, 6, 9, and 12 hours affected the energy gap, which ranges from 2.63 to 2.92 eV. The dye derived from *S. platensis* chlorophyll can effectively absorb visible light and transport electrons to $ZnFe_2O_4$. The soaking time of the anode material has a significant impact on DSSC efficiency, ranging from 76 to 97%.
Key Words: DSSC, dye, microalgae, *Spirulina*, $ZnFe_2O_4$.

Introduction. In the field of material science, there is an advancement in research for the exploration of new materials, and in the course of this, ferrite is one of the most widely developed materials. Subsequently, ferrite possesses a spinel structure denoted by the general formula MFe_2O_4 where M represents a divalent cation of a transition metal (Iyer et al 2009; Satpathy et al 2015; El-Fadl et al 2019; Kamil & Jasim 2020). This compound consists of tetrahedral and octahedral lattice sites, in which there is a distribution of oxygen atoms. The distribution of oxygen atoms in both spaces imparts spinel ferrite with distinctive and unique properties, rendering it promising for a wide range of applications in the health, energy, information technology, environmental, and industrial sectors. Zinc ferrite ($ZnFe_2O_4$) a subtype of spinel ferrite, is a subject of extensive research due to its distinct properties and characteristics (Gestarila & Puryanti 2020). The properties of ferrite are linked to crystallite and grain sizes, which are influenced by the synthesis process and methods employed. $ZnFe_2O_4$ also possesses low magnetic permeability, high magnetic saturation, and potential applications as a nano-absorbent in photodegradation processes (Yao et al 2007; Nurhasanah et al 2012; Suppuraj et al 2017; Dewi et al 2019). Furthermore, $ZnFe_2O_4$ falls into the category of semiconductor materials, with an energy gap ranging from 1.5 to 3.4 eV (Olimpiani & Astuti 2016; Yadav et al 2017; González-Verjan et al 2020; Huerta-Aguilar et al 2022). This classification makes it particularly suitable for applications in the construction of solar cells and dye-sensitized solar cells (DSSC). Subsequently, DSSC represents a set of solar cells based on photoelectrochemical principles, including the transfer of electrons from one phase to another. Unlike traditional solar cells, DSSC separates the processes

of charge separation and light absorption. The DSSC configuration is illustrated in Figure 1 below.

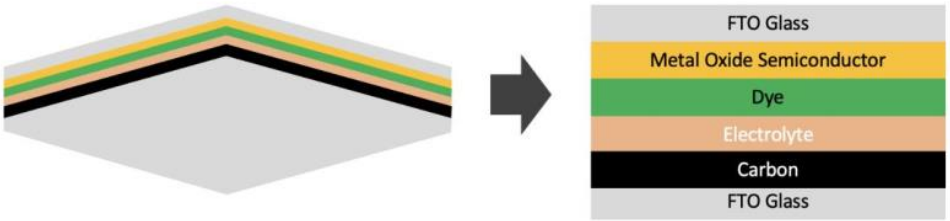

Figure 1. General DSSC configuration.

Dye serves as a light absorber component, while charge separation is carried out by the semiconductor material. The size of the semiconductor particles influences the efficiency level of DSSC where the smaller semiconductor particles coated on the FTO glass layer result in a larger dye absorption area and more excited electrons. Previous research demonstrated the potential of natural dyes as sensitizers in DSSC technology. Additionally, another investigation confirmed the use of TiO_2 nanoparticle semiconductor material in thin layers as an anode in the DSSC configuration. The results showed a crystallite size of 6.93 nm, supporting electron transport and electrolyte species diffusion (González-Verjan et al 2020). The molecular groups in the dye have functional parts coordinated with TiO_2 (Cerdá et al 2022). Subsequently, TiO_2 is one of the functional semiconductor materials with an energy gap of 3.26 to 3.9 eV (Efelina 2017; Indriani et al 2018). Based on the energy gap of TiO_2 and $ZnFe_2O_4$, these compounds are assumed to have the potential to be used as semiconductor materials for application as the cathode in the DSSC configuration.

This research aimed to examine the potential of $ZnFe_2O_4$ as a substrate DSSC technology. The dye material, extracted from *Spirulina platensis* microalgae's chlorophyll (Lim et al 2015), is selected due to its ability to produce photosynthetic pigments like chlorophyll and carotenoids with high efficiency compared to terrestrial plants (Mohammadpour et al 2014). Additionally, *S. platensis* can be produced in large quantities (Orona-Navar et al 2020) and yields carbohydrates and lipids for bioethanol, biohydrogen, and biodiesel production (Masojídek et al 2022). Due to these advantages, *S. platensis* is believed to have the potential as a sensitizer in dye-sensitized solar cells. This research examines the use of chlorophyll extracted from *S. platensis* as a sensitizer in DSSC and explores the optical and dielectric properties of $ZnFe_2O_4$ as an anode as well as its influence on electron transport in DSSC photovoltaic activities. The fabrication of $ZnFe_2O_4$ is carried out using the coprecipitation method based on the relatively uniform size produced.

Material and Method

Fabrication of $ZnFe_2O_4$ nanoparticles. The preparation of $ZnFe_2O_4$ nanoparticles was carried out using the coprecipitation method (Figure 2). The precursors used were zinc chloride hexahydrate ($ZnCl_2.6H_2O$), iron (III) chloride hexahydrate ($FeCl_3.6H_2O$), HCl, and NaOH produced by Merck Emsure. The mass composition of each precursor satisfied the following reaction equation:

$$ZnCl_2 + 2FeCl_3 + 8NaOH + H_2O \rightarrow ZnFe_2O_4 + 8NaCl + 5H_2O$$

The coprecipitation process started by creating a salt solution from $FeCl_3.6H_2O$ and $ZnCl_2.6H_2O$ precursors. A specific amount of each precursor's mass was dissolved in 25 mL of distilled water and stirred at room temperature for 3 minutes at 500 rpm. Once the $ZnCl_2$ and $FeCl_3$ solutions were formed, both solutions were mixed, then 3.37 mL of HCl was added and stirred at 500 rpm for 3 minutes.

The solution was subsequently slowly introduced drop by drop into a stirring NaOH solution, operating at 1000 rpm, while maintaining a temperature of 95°C, using a buret

for 60 minutes. The resulting precipitate was left for 1 hour and washed using distilled water to reduce the soluble salt content. After the washing process, a dark brown wet precipitate (slurry) was obtained and then heated in an oven at 100°C for 4 hours. The heating process yielded solid pieces from the slurry, which were then ground into fine grains and proceeded to the characterization stage.

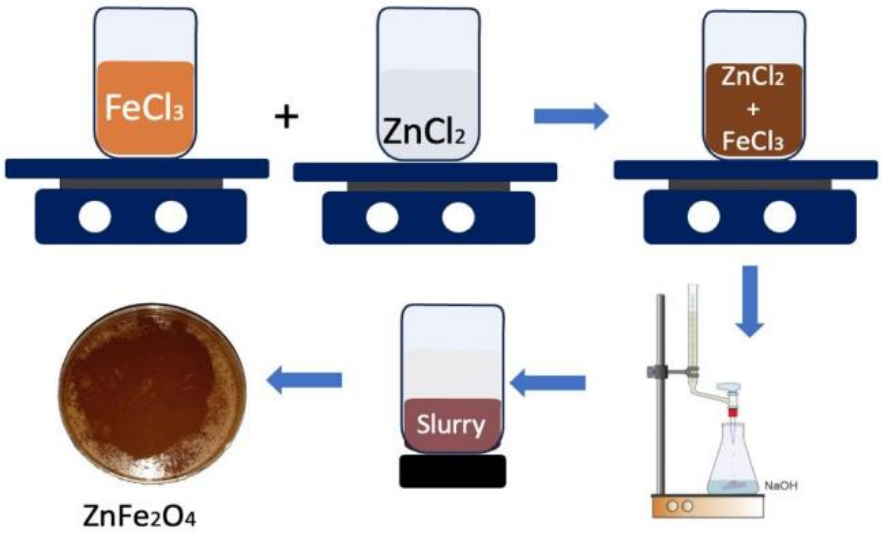

Figure 2. Coprecipitation method.

Extraction of Spirulina chlorophyll. The extraction of *S. platensis* chlorophyll included the filtration of 250 mL of alga using Whatman Grade 1 filter paper. This filtration resulted in wet *S. platensis* biomass, which was dried at room temperature, yielding 0.3 g or 30 mg of dry biomass. Furthermore, this dry biomass was soaked (macerated) in a 10 mL acetone solution to extract the chlorophyll in the sample. The resulting solution underwent centrifugation for 20 minutes at a speed of 3000 rpm to separate the precipitate from the supernatant. The supernatant obtained served as the dye obtained from *S. platensis* chlorophyll for application in DSSC.

Fabrication and configuration of DSSC. The preparation of the DSSC substrate started with a thorough cleaning of a 2.5 x 2.5 cm FTO glass using a combination of distilled water and ethanol, followed by approximately 5 minutes of sonication. Non-conductive areas were meticulously isolated along the edges of the FTO glass, and the central area measuring 1 x 1 cm was then substituted with a paste consisting of $ZnFe_2O_4$ (Figure 3).

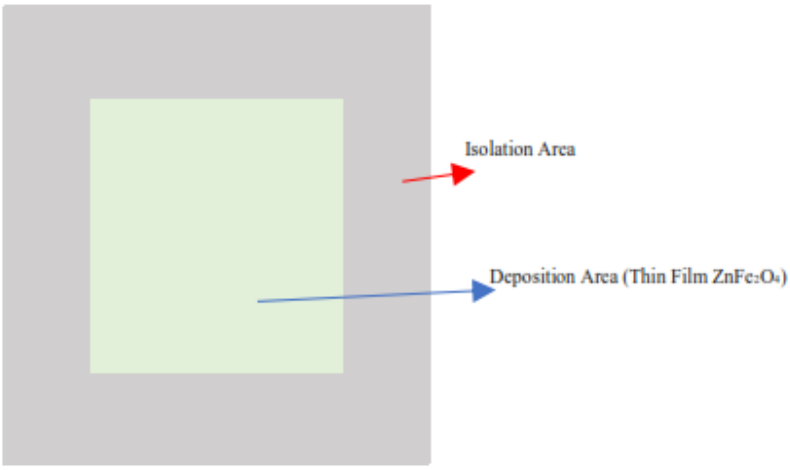

Figure 3. Deposition and isolation areas.

The paste was prepared by dissolving 0.2 g of PVA in 20 mL of distilled water and stirring at 80°C with a speed of 500 rpm for 10 minutes. Once the PVA paste was formed, 1 g of $ZnFe_2O_4$ powder was added and stirred using a spatula for 2 minutes, followed by stirring at 1000 rpm at room temperature for 30 minutes. After preparing the $ZnFe_2O_4$ paste, the deposition stage on the FTO glass was carried out using a spin-coater at a speed of 1000 rpm for 2 minutes. Subsequently, it was air-dried at room temperature for 15 minutes and further dried in an oven at 150°C for 30 minutes. The FTO glass coated with $ZnFe_2O_4$ was immersed in 5 mL of *S. platensis* chlorophyll supernatant (dye) for 12 hours in dark conditions (no light) and proceeded to the drying stage for 10 hours at room temperature. The counter-electrode preparation included using carbon derived from candle soot on the conductive area of the FTO glass, which was then smoothed using a tissue soaked in methanol on a 2 x 2 cm area of the 2.5 x 2.5 cm glass. The assembly of the DSSC follows the sandwich configuration shown in Figure 4. The arrangement sequence consists of FTO glass coated with $ZnFe_2O_4$ paste, dye, and iodine as the electrolyte solution, carbon, and FTO glass.

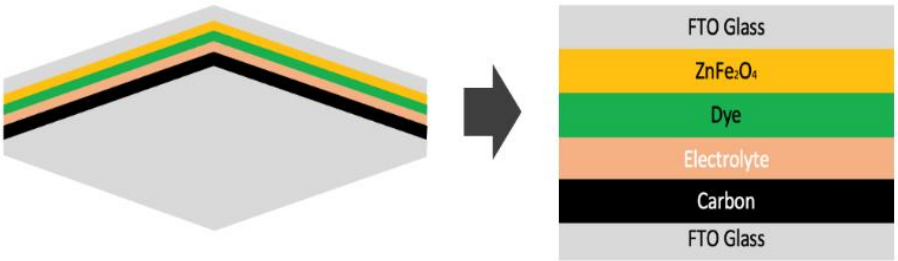

Figure 4. DSSC configuration.

Results

X-Ray diffraction analysis. The crystallite size and lattice parameters are determined through XRD analysis. The characterization results are presented in Figure 5 below.

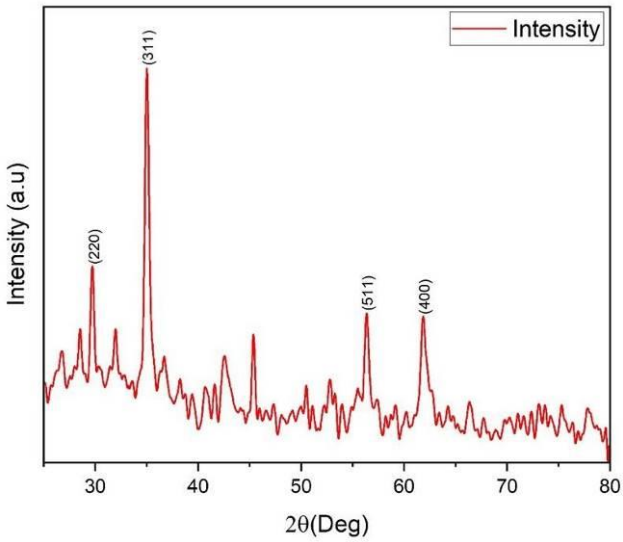

Figure 5. X-Ray diffraction diffractogram.

The XRD graph shows that the $ZnFe_2O_4$ nanoparticles possess polycrystalline properties (Cao 2021). This characterization result is marked by the identification of more than one Bragg plane peak. The diffraction peaks obtained are 220, 311, 511, and 440, in line with JCPDS PDF Card No 01-1108 data. The crystallite size and lattice parameter can be calculated using the following equations 1 and 2:

$$D = \frac{0.9\lambda}{B\cos\theta} \quad \text{(eq. 1)}$$

$$\alpha = \frac{\lambda}{2\sin\theta}\sqrt{h^2 + k^2 + l^2} \quad \text{(eq. 2)}$$

where λ indicates the X-ray wavelength, B is the Full Width at Half Maximum (FWHM) value, θ denotes the diffraction angle, and α informs the lattice parameter.

The calculation results of the crystallite size and lattice parameter are presented in Table 1.

Table 1

XRD analysis of $ZnFe_2O_4$

Peak	*2θ*	*λ*	*FWHM*	*θ*	*k*	*t(nm)*	*±Δt*	*a (nm)*	*±Δa*
220	29.72	1.5406	0.37	14.86	0.9	22.21	0.02	0.850	0.001
311	35.02	1.5406	0.48	17.51	0.9	17.35	0.01	0.849	0.001
511	56.36	1.5406	0.47	28.18	0.9	19.18	0.07	0.848	0.003
440	61.92	1.5406	0.79	30.96	0.9	11.73	0.06	0.847	0.004

The crystallite size of $ZnFe_2O_4$ obtained ranges from 11.73 to 22.21 nm, which is similar to the findings from previous research (Yadav et al 2017). Furthermore, the lattice parameter obtained is in the range of 0.84-0.85 nm, closely in line with the results reported in other investigations using different methods (Sai et al 2015). The non-uniform crystallite size produced may indicate the presence of crystal defects (strain), causing a transition in the atom positions within the sub-lattice, reflected by the variation in diffraction peak heights (Putra et al 2023), where higher diffraction peak shows an accumulation of atoms within the plane. These atoms are distributed across 2 sub-lattices: tetrahedral (site-A) and octahedral (site-B) (Patade et al 2020). The radius of site-A and site- B can be calculated using equations 3 and 4 below:

$$rA = [C_{Zn}r(Zn^{2+}) + C_{Fe}r(Fe^{3+})] \quad \text{(eq. 3)}$$

$$rB = 1/2\ [C_{Zn}r(Zn^{2+}) + C_{Fe}r(Fe^{3+})] \quad \text{(eq. 4)}$$

where C represents the concentrations of each element Zn and Fe, while r is the ionic radius.

From the calculations of equations 3 and 4, the theoretical lattice parameter for $ZnFe_2O_4$ can be calculated using equation 5 below:

$$\alpha_{th} = \frac{8}{3\sqrt{3}}[(rA + r0) + \sqrt{3}(rB + r0)] \quad \text{(eq. 5)}$$

The theoretical lattice parameter is symbolized by α_{th}, and r0 is the radius of an oxygen atom (r0 = 0.138). The difference between the experimental (Table 1) and theoretical (α_{th}) lattice parameter values are assumed to be influenced by the oxygen atom as the anion parameter (u). The positions of these atoms can be influenced by the synthesis process, including the method, mass composition of each compound, and the synthesis temperature. The anion parameter can be calculated using equation 6 below:

$$u = [(rA + r0)\frac{1}{\sqrt{3a}} + \frac{1}{4}] \quad \text{(eq. 6)}$$

The magnitude of the uideal parameter is 0.375, and the change in the u value is represented by Δ (equation 7). The larger the value Δ, the greater the shift in the position of atoms in the crystal structure, resulting in crystal defects (strain):

$$\Delta = |u - u_{ideal}| \quad \text{(eq. 7)}$$

The calculation results of rA, rB, ath, u, and Δ are shown in Table 2.

Table 2

Microstructure analysis information

Peak	*rA*	*rB*	α_{th}	*Uideal*	*U*	*Δ*
220	1.52	1.22	6.17	0.375	0.3627	0.0123
311	1.52	1.22	6.17	0.375	0.3627	0.0123
511	1.52	1.22	6.17	0.375	0.3629	0.0121
440	1.52	1.22	6.17	0.375	0.3630	0.0120

Table 2 shows that the crystal structure produced exhibits some crystal defects as indicated by the deviation in the positions of oxygen atoms. However, the deviation is not significant because to achieve the ideal parameter, the lattice parameter produced falls within standard deviation tolerance. In Figure 5, some diffraction peaks that are not identified with the JCPDS PDF Card No. 01-1108 database also appear. The presence of these peaks can be considered as noise in the identification process, but they cannot be ignored because they can affect the properties of the resulting material. Furthermore, the presence of these noise peaks is caused by the heating factor applied at a low temperature (Anggraini et al 2021).

Discussion

Optical properties. The UV-Vis characterization results of the $ZnFe_2O_4$ sample are shown in Figure 6 below:

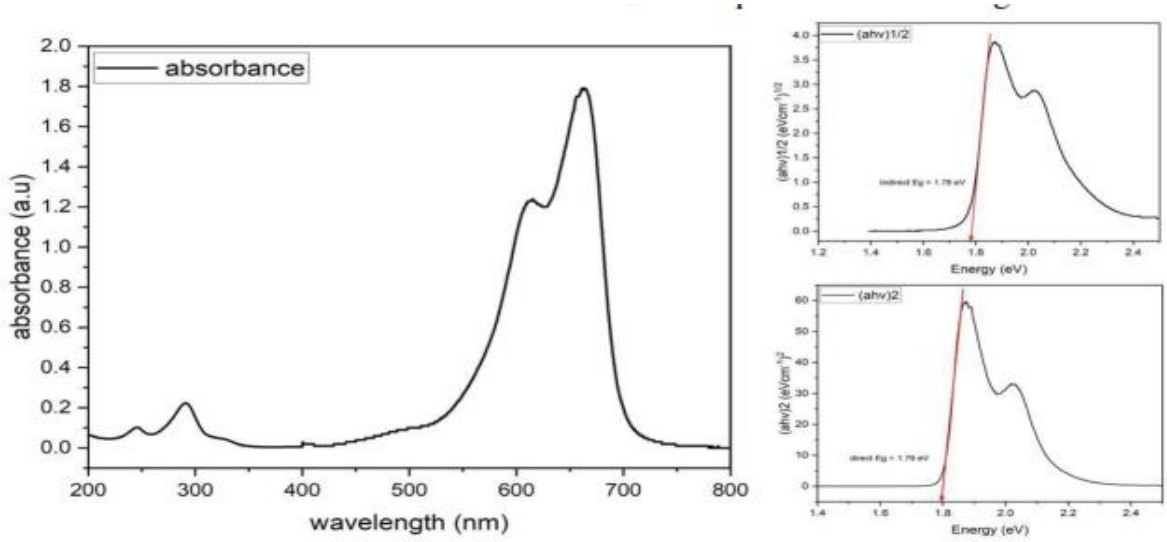

Figure 6. Absorbance spectrum of $ZnFe_2O_4$ nanoparticles.

In Figure 6, the absorbance spectrum is observed within the wavelength range of 200 to 800 nm. This phenomenon indicates the excitation of electrons from the conduction band to the valence band. A higher absorption peak implies a greater number of free electrons undergoing transitions between energy bands (band-to-band transitions). The transition of electrons between valence bands is influenced by the energy in the optical gap. Figure 6 shows an energy gap of 1.79 eV for the direct gap and 1.78 eV for the indirect gap, which is in line with previous research findings (Huerta-Aguilar et al 2022). The direct gap represents the minimum energy required by free electrons to move from the highest energy state of the valence band to the lowest energy state of the conduction band with the same momentum vector, influencing electrons that can directly emit photons. The indirect gap is the energy required to move electrons between bands with different momentum vectors, hence in the electron transition process, atoms absorb both photon and phonon energy (Figure 7).

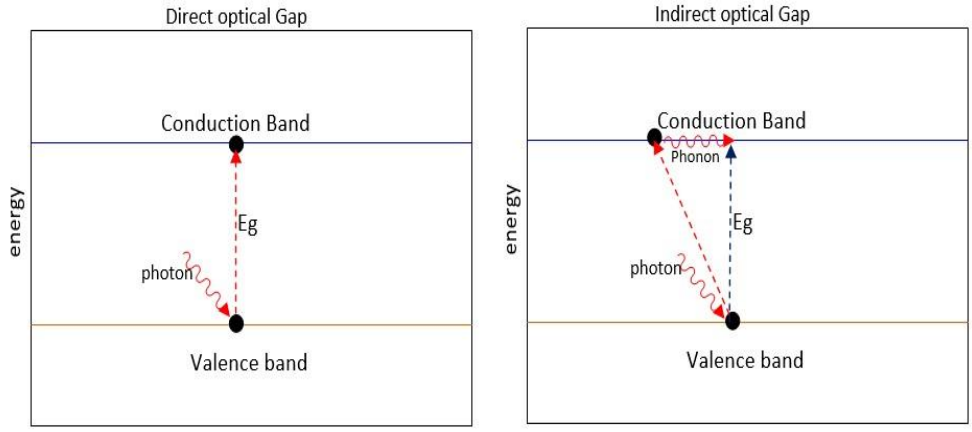

Figure 7. Direct and indirect gap phenomena.

The calculation of the energy gap (direct and indirect) uses Touch's plot method (Yakob et al 2019). The results show that direct and indirect gap energies tend to be the same. Subsequently, the width of the absorption peak is correlated with the crystallite size of the nanoparticles produced. The larger the crystallite size, the larger the optical gap energy produced. This is because the optical gap energy is influenced by the number of electrons from the constituent atoms of the crystallite lattice. Another factor influencing the optical gap energy is lattice distortion, which causes crystal imperfections (strain) (Mondal et al 2019). This distortion causes crystal imperfections, leading to shifts in atom positions, electron positions, and interactions within the crystal. These alterations create a boundary between the conduction band and valence band, a phenomenon known as band tailing (Mistrik et al 2017). Band tailing is assumed to be the end of the valence band, which has the highest electron density below the conduction band. The width of the energy at the band edge is known as the Urbach energy.

Optical properties of S. platensis microalgae. The UV-Vis spectrum of *S. platensis* microalgae is shown in Figure 8. In Figure 8, two absorption peaks are visualized at a wavelength of 428 nm and 665 nm respectively.

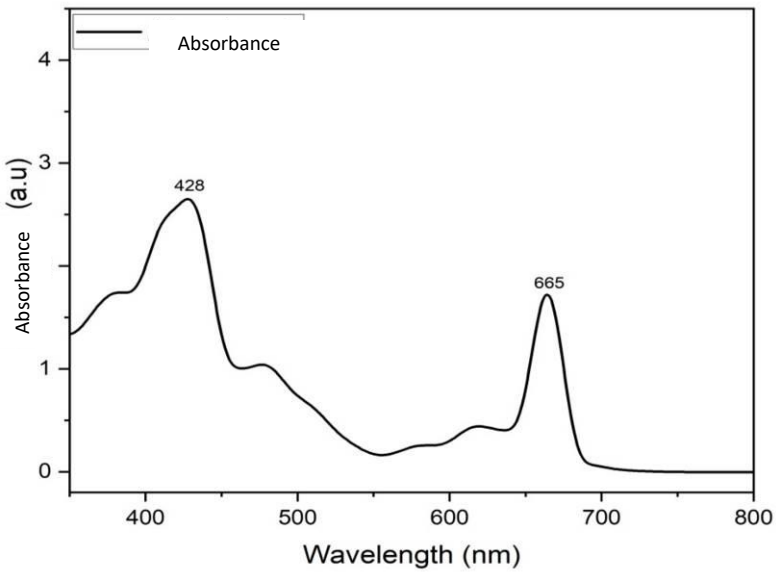

Figure 8. Chlorophyll UV-Vis spectrum.

The absorption peaks in chlorophyll reveal the presence of two distinct types of molecules, namely chlorophyll a (665 nm) and chlorophyll b (425 nm). These peaks correspond to the results reported in previous research (Orona-Navar et al 2020;

Masojídek et al 2022). The chlorophyll found in *S. platensis* can be used as a sensitizer due to its ability to absorb visible light. The UV-Vis characterization on the $ZnFe_2O_4$ anode layer, influenced by the soaking time in the dye, is shown in Figure 9. The absorbance capability is measured for 12 hours with variations of 3, 6, 9, and 12 hours (Figure 9).

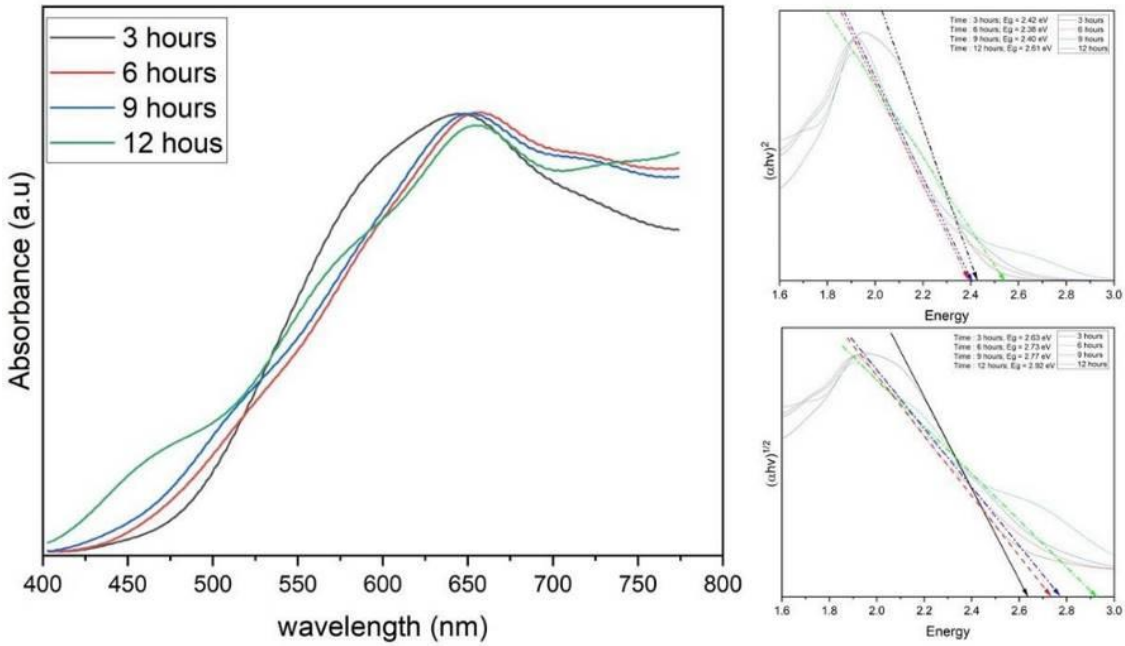

Figure 9. Energy gap spectrum toward soaking time.

In Figure 9, the highest absorption peak is evident between the soaking times of 3 to 9 hours. However, beyond 9 hours, the dye exhibits a reduction in absorbance. The decrease in the absorption peak influences the increase in the energy gap of $ZnFe_2O_4$ coated with dye. The increase in the energy gap results in electrons having difficulty transitioning from one energy band state to another, requiring more energy to stimulate the electrons to transition from one state to another.

Photoelectric characterization of DSSC. The characterization of Current (I) and Voltage (V) is performed under direct sunlight illumination. The system consists of cables, a voltmeter, a variable resistor, and the $ZnFe_2O_4$/dye electrode side (Figure 10).

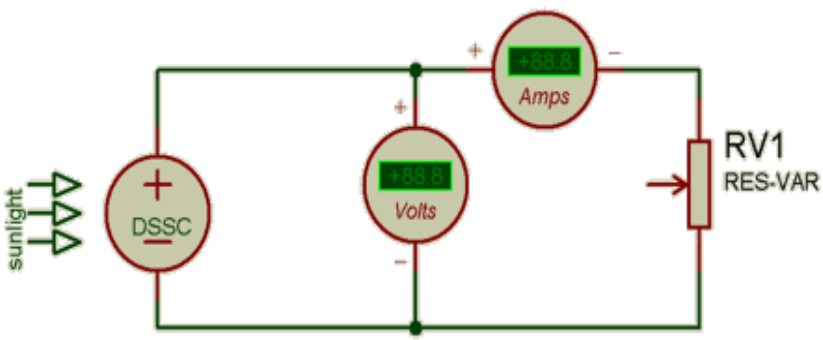

Figure 10. DSSC testing circuit.

Voltage measurement is carried out by applying maximum load to the circuit (maximum R) and subsequently reducing the resistance to approach 0. At each step of the load application, the voltage and current generated are recorded. Photovoltaic conversion efficiency is calculated using the following equation 8:

$$\eta = \frac{FF \times I_{SC} \times V_{OC}}{P_{in}} \times 100 \quad \text{(eq. 8)}$$

$$FF = \frac{I_{max} \times V_{max}}{I_{SC} \times V_{OC}} \quad \text{(eq. 9)}$$

where η represents photovoltaic efficiency, FF is the fill factor (eq. 9), Isc is the short-circuit current density, Voc indicates the voltage at an open circuit, and Pin is the sunlight intensity (117 mW/cm^2).

The results of current (I) and Voltage (V) characterization toward soaking time are shown in Figure 11.

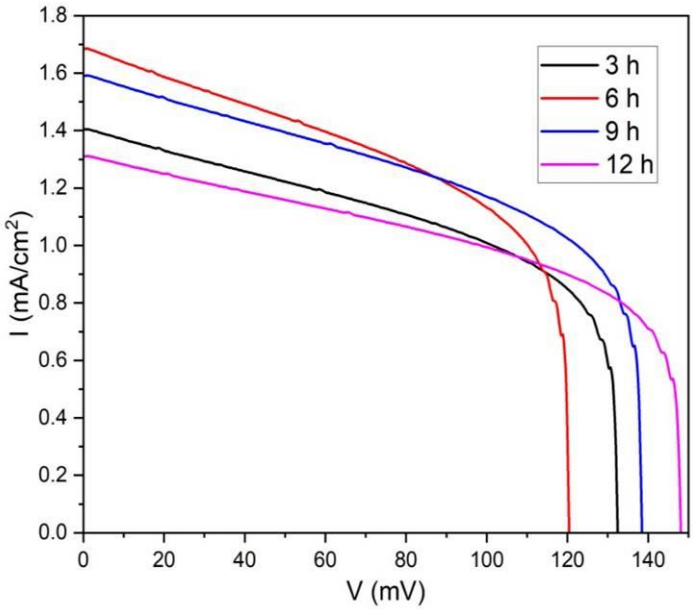

Figure 11. Current (I) voltage (V) characterization of $ZnFe_2O_4$/dye.

Figure 11 presents the information on the characteristics of current (I) and voltage (V) measured on the $ZnFe_2O_4$ anode immersed in the dye for 3, 6, 9, and 12 hours with anobservation cell area of 1 cm^2. The power conversion efficiency of DSSC is shown in Table 3.

Table 3

DSSC sensitizer para,eters with different soaking times

Sample	*Time*	V_{OC} *(mV)*	I_{SC} *(mA)*	V_{max} *(mV)*	I_{max} *(mA)*	*η%*	*FF*
A	3 hours	132.44	1.40	127.32	0.70	76	0.48
B	6 hours	120.38	1.69	108.91	1.02	95	0.55
C	9 hours	138.41	1.59	131	0.86	97	0.51
D	12 hours	148.06	1.03	143.64	0.63	77	0.59

Table 3 presents the information on DSSC efficiency, ranging from 76 to 97%. The highest efficiency is found in sample C at 97% with a current density of 1.59 mA/cm^2, slightly lower than B at 1.69 mA/cm^2 with an efficiency of 95%. The magnitude of the current density in each sample is assumed to be influenced by the energy gap of each sample. The larger the energy gap, the more energy is required to excite electrons from the valence band to the conduction band, and vice versa. The soaking time also plays a role in determining the number of electrons undergoing excitation. It is assumed that electrons at the interface between the $ZnFe_2O_4$ material interact with electrons in the dye. When dye absorbs energy from the sun, it transfers electrons to the carbon layer through the electrolyte, which is a conductor, resulting in the generation of electric current. Moreover, the high solar cell efficiency is also attributed to the role of chlorophyll as a molecule that absorbs light in maintaining the photosystem structure (Figure 12).

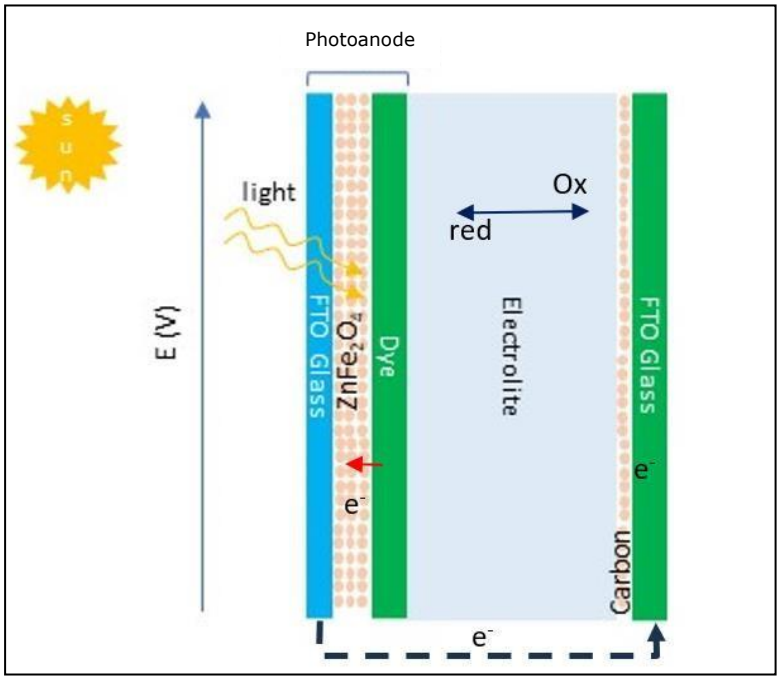

Figure 12. Electron transport process in DSSC.

Figure 12 shows the phenomenon of sunlight absorption by chlorophyll, depicting the process of exciting electrons from the ground state to the excited state. It further demonstrates the efficient transfer of absorbed energy to the dye, enabling the dye to inject electrons into the conduction band of $ZnFe_2O_4$. Subsequently, these electrons are then passed through FTO glass to the counter electrode.

Conclusions. $ZnFe_2O_4$ was successfully synthesized using the coprecipitation method, resulting in a polycrystalline material with a crystallite size ranging from 11.73 nm to 22.21 nm. The material showed an energy gap of 1.78 to 1.79 eV, making it a promising choice as a photoanode material in the DSSC configuration. The UV-Vis characterization results showed that $ZnFe_2O_4$soaked with dye for 3, 6, 9, and 12 hours has an impact on the energy gap, ranging from 2.63 to 2.92 eV. The dye produced from spirulina microalgae chlorophyll showed the ability to absorb visible light and carry out electron transport to $ZnFe_2O_4$. The soaking time of the anode material has an impact on DSSC efficiency which ranges from 76% to 97%. Generally, the DSSC efficiency involving the dye consistently exceeds 70%, indicating the promise of this configuration for solar energy conversion.

Use of AI tools declaration. The authors declare they have not used Artificial Intelligence (AI) tools in the creation of this article.

Acknowledgements. This research was funded by 1. Universitas Syiah Kuala, the Ministry of Education, Culture, Research, and Technology, following the Research Professor Contract for the Fiscal Year 2023, Contract Number 57/UN11.2.1/PT.01.03/PNBP/2023, 2. Ministry of Education, Culture, Research, and Technology, following the Research Contract for the fiscal year 2023, Contract Number 168/E5/PG.02.00.PL/2023**.**

Conflict of interest. The authors declare that there is no conflict of interest.

References

Anggraini V., Putra R. A., Fadlly T. A., 2021 Synthesis and characterization of manganese ferrite ($MnFe_2O_4$) nanoparticles by coprecipitation method at low temperatures. Advances in Social Science, Educations and Humanities Research 576:118-122.

Cao X., 2021 Zinc ferrite nanoparticles: Simple synthesis via lyophilisation and electrochemical application as glucose biosensor. Nano Express 2:024001.

Cerdá M. F., 2022 Dyes from the southern lands: an alternative or a dream? Solar 2(4): 519-539.

Dewi L. R., Widanarto W., Effendi M., 2019 [Effect of sintering temperature on composition, magnetic properties and microwave absorption of zinc-ferrite nanocomposites]. Jurnal Teras Fisika 2(1):18-21. [in Indonesian]

Efelina V., 2017 [Preparation and study of gap energy TiO_2:Cu thin film fabricated by spin coating technique]. Jurnal Pendidikan Fisika dan Keilmuan 3(1):19-27. [in Indonesian]

El-Fadl A. A., Hassan A. M., Mahmoud M. H., Tatarchiuk T., Yaremiy I. P., Gismelssed A. M., Ahmed M. A., 2019 Synthesis and magnetic properties of spinel $Zn_{1-x}Ni_xFe_2O_4$ ($0.0 \leq x \leq 1.0$) nanoparticles synthesized by microwave combustion method. Journal of Magnetism and Magnetic Materials 471:192-199.

Gestarila C., Puryanti D., 2020 [Synthesis of zinc ferrite nanoparticles ($ZnFe_2O_4$) using the coprecipitation method and characterization of their crystal structure]. Jurnal Fisika Unand 9(3):299-303. [in Indonesian]

González-Verjan V. A., Trujillo-Navarrete B., Félix-Navarro R. M., Díaz de León J. N., Romo-Herrera J. M., Calva-Yáñez J. C., Hernández-Lizalde J. M., Reynoso-Soto E. A., 2020 Effect of TiO_2 particle and pore size on DSSC efficiency. Materials for Renewable and Sustainable Energy 9(2):1-8.

Huerta-Aguilar C. A., Diaz-Puerto Z. J., Tecuapa-Flores E. D., Thangarasu P., 2022 Crystal plane impact of $ZnFe_2O_4$-Ag nanoparticles influencing photocatalytical and antibacterial properties: experimental and theoretical studies. ACS Omega 7(38): 33985-34001.

Indriani D., Fahyuan H. D., Ngatijo N., 2018 [Test Uv-Vis layer Tio_2/N_2 for determining band gap energy]. Journal Online of Physics 3(2):6-10. [in Indonesian]

Iyer R., Desai R., Upadhyay R. V., 2009 Low-temperature synthesis of nanosized $Mn_{1-x}Zn_xFe_2O_4$ ferrites and their characterizations. Bulletin of Materials Science 32(2): 141-147.

Kamil M. K., Jasim K. A., 2020 Calculating of crystalline size, strain, and degree of crystallinity of the compound ($HgBa_2Ca_2Cu_3O_{8+\sigma}$) by different method. IOP Conference Series: Materials Science and Engineering 928:072109.

Lim A., Manaf N. H., Tennakoon N., Chandrakanthi R. L. N., Lim L. B. L., Bandara J. M. R. S., Ekanayake P., 2015 Higher performance of DSSC with dyes from *Cladophora* sp. as mixed cosensitizer through synergistic effect. Journal of Biophysics 2015:510467.

Masojídek J., Gomez-Serrano C., Ranglova K., Cicchi B., Bogeat A. E., et al., 2022 Photosynthesis monitoring in microalgae cultures grown on municipal wastewater as a nutrient source in large-scale outdoor bioreactors. Biology 11(10):1380.

Mistrik J., Kasap S., Ruda H. E., Koughia C., Singh J., 2017 Optical properties of electronic materials: fundamentals and characterization. In: Springer handbook of electronic and photonic materials. Kasap S., Capper P. (eds), Springer International Publishing, pp. 47-83.

Mohammadpour R., Janfaza S., Abbaspour-Aghdam F., 2014 Light harvesting and photocurrent generation by nanostructured photoelectrodes sensitized with a photosynthetic pigment: a new application for microalgae. Bioresource Technology 163:1-5.

Mondal D. K., Borgohain C., Paul N., Borah J. P., 2019 Tuning hyperthermia efficiency of $MnFe_2O_4$/ZnS nanocomposites by controlled ZnS concentration. Journal of Materials Research and Technology 8(6):5659-5670.

Nurhasanah I., Sutanto H., Muhlisin Z., Nurdianik A. A. S., Nursanti I., 2012 [Synthesis of cerium oxide nanoparticles using the precipitation method and their optical properties]. Berkala Fisika 15(2):41-48. [in Indonesian]
Olimpiani I., Astuti, 2016 [Effect of alkali compound doping on the energy band gap of ZnO nanoparticles]. Jurnal Fisika Unand 5(2):115-121. [in Indonesian]
Orona-Navar A., Aguilar-Hernández I., López-Luke T., Pacheco A., Ornelas-Soto N., 2020 Dye sensitized solar cell (DSSC) by using a natural pigment from microalgae. International Journal of Chemical Engineering and Applications 11(1):14-17.
Patade S. R., Andhare D. D., Kharat P. B., Humbe A. V., Jadhav K. M., 2020 Impact of crystallites on enhancement of bandgap of $Mn_{1-x}ZnxFe_2O_4$ ($1 \geq x \geq 0$) nanospinels. Chemical Physics Letters 745:137240.
Putra R. A., Fadlly T. A., Asmara V., Monica D., Sartika et al., 2023 The effect of Zn^{2+} ion substitution on nanoparticles of $Zn_xMn_{(1-X)}Fe_2O_4$ (X = 0.2, 0.4, 0.6, 0.8) towards signal surface plasmon resonance (SPR). Materials Research Innovations 27(6): 420-428.
Sai R., Kulkarni S. D., Bhat S. S. M., Sundaram N. G., Bhat N., Shivashankar S. A., 2015 Controlled inversion and surface disorder in zinc ferrite nanocrystallites and their effects on magnetic properties. RSC Advances 5(14):10267-10274.
Satpathy M. P., Moharana B. R., Dewangan S., Sahoo S. K., 2015 Modeling and optimization of ultrasonic metal welding on dissimilar sheets using fuzzy based genetic algorithm approach. Engineering Science and Technology, an International Journal 18(4):634-647.
Suppuraj P. S., Thirunarayanan G., Swaminathan M., Muthuvel I., 2017 Facile synthesis of spinel nanocrystalline $ZnFe_2O_4$: enhanced photocatalytic and microbial applications. Materials Science and Applied Chemistry 34(1):5-11.
Yadav R. S.., Kuřitka I., Vilcakova J., Urbánek P., Machovsky M., Masař M., Holek M., 2017 Structural, magnetic, optical, dielectric, electrical and modulus spectroscopic characteristics of $ZnFe_2O_4$ spinel ferrite nanoparticles synthesized via honey-mediated sol-gel combustion method. Journal of Physics and Chemistry of Solids 110:87-99.
Yakob M., Umar H., Wahyuningsih P., Putra R. A., 2019 Characterization of microstructural and optical $CoFe_2O_4/SiO_2$ ferrite nanocomposite for photodegradation of methylene blue. AIMS Materials Science 6(1):45-51.
Yao C., Zeng Q., Goya G. F., Torres T., Liu J., Wu H., Ge M., Zeng Y., Wang Y., Jiang J. Z., 2007 $ZnFe_2O_4$nanocrystals: synthesis and magnetic properties. The Journal of Physical Chemistry C 111(33):12274-12278.

Received: 23 March 2024. Accepted: 30 May 2024. Published online: 30 June 2024.
Authors:
Razali Thaib, Mechanical Engineering Department, Faculty of Engineering, Universitas Syiah Kuala (USK), Syeh Abdurrauf Street, No. 7, Darussalam, Banda Aceh, 23111, Indonesia, e-mail: razalithaib@usk.ac.id
Hamdani Umar, Mechanical Engineering Department, Faculty of Engineering, Universitas Syiah Kuala (USK), Syeh Abdurrauf Street, No. 7, Darussalam, Banda Aceh, 23111, Indonesia, e-mail: hamdani@unsyiah.ac.id
Mulia Safrida Sari, Biology Study Program, Faculty of Engineering, Universitas Samudra, Aceh, Indonesia, e-mail: muliasari03@unsam.ac.id
Rachmad Almi Putra, Physics Study Program, Faculty of Engineering, Universitas Samudra, Aceh, Indonesia, e-mail: rachmad.almi@unsam.ac.id

How to cite this article:
Thaib R., Umar H., Sari M. S., Putra R. A., 2024 Fabrication of zinc ferrite ($ZnFe_2O_4$) as a photoanode layer on dye-sensitized solar cells from *Spirulina platensis*. AES Bioflux 16(1):1-12.